The response of internal dynamics to hydrophobic core mutations in the SH3 domain from the Fyn tyrosine kinase

ANTHONY MITTERMAIER[1] AND LEWIS E. KAY[1,2]

[1]Department of Biochemistry and [2]Departments of Medical Genetics and Chemistry, University of Toronto, Toronto, Ontario, Canada M5S 1A8

(RECEIVED October 31, 2003; FINAL REVISION December 24, 2003; ACCEPTED December 29, 2003)

Abstract

We have used ^{15}N- and ^{2}H-NMR spin relaxation experiments to study the response of backbone and side-chain dynamics when a leucine or valine is substituted for a completely buried phenylalanine residue in the SH3 domain from the Fyn tyrosine kinase. Several residues show differences in the time scales and temperature dependences of internal motions when data for the three proteins are compared. Changes were also observed in the magnitude of dynamics, with the valine, and to a lesser extent leucine mutant, showing enhanced flexibility compared to the wild-type (WT) protein. The motions of many of the same amide and methyl groups are affected by both mutations, identifying a set of loci where dynamics are sensitive to interactions involving the targeted side chain. These results show that contacts within the hydrophobic core affect many aspects of internal mobility throughout the Fyn SH3 domain.

Keywords: NMR relaxation; hydrophobic core; site-directed mutagenesis; protein dynamics

Most native globular proteins have well-ordered three-dimensional configurations and interiors with packing densities similar to those of organic crystals (Richards 1974; Chothia 1975). In contrast, many designed proteins are highly mobile, as evidenced by rapid amide hydrogen exchange and broadened NMR spectra with narrow chemical shift dispersion, even when they exhibit cooperative folding transitions and possess unique overall topologies (Handel et al. 1993; Davidson et al. 1995; Isogai et al. 1999). The tightness of packing in the hydrophobic core is thought to be a major determinant of whether a protein will adopt a specific, native-like fold or a more heterogeneous ensemble of compact conformations (Woolfson 2001; Isogai et al. 2002). Several designed proteins in which side-chain contacts were exhaustively optimized using a computer algorithm have highly ordered structures (Dahiyat and Mayo 1997a; Offredi et al. 2003). Conversely, repacked core mutants of the β1 domain from protein G exhibit increased amide hydrogen exchange and decreased chemical shift dispersion in NMR spectra when the total volume of core residues is increased beyond that of the WT (Dahiyat and Mayo 1997b). Cavity mutants of proteins also often have significantly increased dynamics. For example, the L99A mutant of T4 lysozyme was shown to be much more mobile than the WT protein on a millisecond time scale (Mulder et al. 2001).

Here, we have examined the extent to which conservative amino acid substitutions in the hydrophobic core influence protein flexibility by using ^{15}N- and ^{2}H-NMR spin relaxation experiments to measure the magnitude of nanosecond to picosecond time scale motions in the WT and two single-site mutants of the SH3 domain from the Fyn tyrosine kinase. In addition to monitoring the rates of decay of longitudinal and transverse deuterium magnetization in $^{13}CH_2D$ methyl groups, we have measured the relaxation of three additional deuterium magnetization operators using experiments recently developed in our laboratory (Millet et al. 2002). We have further extended our investigation by performing ^{15}N relaxation experiments at four temperatures

Reprint requests to: Anthony Mittermaier or Lewis E. Kay, Departments of Biochemistry, Chemistry and Medical Genetics, University of Toronto, Toronto, Ontario, Canada M5S 1A8; e-mail: tmitter@pound.med.utoronto.ca or kay@pound.med.utoronto.ca; fax: (416) 978-6885.

Article and publication are at http://www.proteinscience.org/cgi/doi/10.1110/ps.03502504.

ranging from 5°C to 35°C. The temperature dependence of internal motions is related to the heat capacity of the folded protein that can influence its resistance to thermal denaturation (Seewald et al. 2000).

Results

Thermodynamic and structural effects of F20L and F20V mutations on the Fyn SH3 domain

SH3 domains are small (≈60 aa) modular mediators of protein–protein interactions that adopt β-sandwich folds (Musacchio et al. 1994). Detailed analysis of SH3 domain sequence and structural alignments (Larson and Davidson 2000) has identified 10 conserved hydrophobic core positions including residue 20, located in the RT-Src loop, which is, on average, 2% exposed to solvent. Phenylalanine, with a side-chain volume of 140 $Å^3$, occurs at this position in the WT Fyn sequence. Substitution of Phe 20 with leucine (115 $Å^3$) and valine (100 $Å^3$) reduces the thermodynamic stability of this domain by 1.11 kcal/mole and 1.88 kcal/mole, respectively, as calculated from folding/unfolding kinetics experiments (Northey et al. 2002). Differences in H_2O/octanol transfer free energies, 0.13 kcal/mole and 0.77 kcal/mole for phenylalanine-leucine and phenylalanine-valine (Fauchere and Pliska 1983; Karplus 1997), partially but not completely account for the destabilizing effects of the F20L and F20V mutations. The additional losses of stability are most likely due to disruptions of core packing. Mutants in which buried side-chain volume is decreased usually retain packing defects (Richards and Lim 1994), and loss of van der Waals interaction energies has been identified as a major factor in the reduced stability of such proteins (Eriksson et al. 1992; Lee and Shin 2000). Here we present a detailed dynamics study of the WT Fyn SH3 domain and a pair of single mutants with amino acid substitutions at the same site. In this manner, the loss of van der Waals interactions involving position 20 can be characterized in terms of changes in dynamics without complicating effects that would likely arise if the WT protein were compared with mutants containing a larger number of substitutions (Johnson and Handel 1999).

The structure of the human Fyn SH3 domain has been solved by X-ray crystallography (Noble et al. 1993) and NMR (Morton et al. 1996); however, neither the structure of the chicken isoform of this domain which was used in this investigation, nor the structures of the F20L or F20V mutants have been determined experimentally. Note that the chicken isoform was chosen for analysis because a significant body of thermodynamic and mutational data has been accumulated for this form of the protein (Northey et al. 2002; Di Nardo et al. 2003). To assess the effects of the mutations on the structure of the SH3 domain, one-bond backbone ^{15}N-^{1}H residual dipolar couplings ($^{1}D_{NH}$) were measured for the F20L, F20V, and WT proteins, oriented with respect to the static magnetic field using a suspension of Pf1 bacteriophage particles (Hansen et al. 1998). Residual dipolar couplings are sensitive to the orientations of internuclear vectors within the molecular frame and conformational changes that reorient NH bond vectors can lead to large changes in $^{1}D_{NH}$ values. The dipolar couplings measured for WT, F20L, and F20V proteins are compared in Figure 1A,B. Virtually identical values are obtained for all three molecules, indicating that the overall backbone structure of the Fyn SH3 domain is essentially unaffected by the F20L and F20V mutations. These results are in agreement with those of other studies, which show that nondisruptive (volume-reducing, hydrophobic to hydrophobic) mutations generally do not affect the overall protein fold (Eriksson et al. 1992; Buckle et al. 1996; De Vos et al. 2001).

$^{1}D_{NH}$ values for the WT protein (chicken isoform) were fit to the X-ray crystal structure (human isoform), yielding alignment tensor parameters, $A_a = 4.4 \times 10^{-4}$ and $R = 0.66$. A comparison of predicted and experimental couplings produces a correlation coefficient of 0.95 and a quality factor, $Q = 0.31$. This represents poorer agreement than would be predicted based on the resolution of the crystal structure, 1.9 Å (Noble et al. 1993), because experimental and predicted dipolar couplings obtained with structures at this resolution typically yield Q factors of 0.20 to 0.25 (Bax 2003). The discrepancy is unlikely to be due to experimental errors in the dipolar couplings because WT and mutant data are in extremely good agreement, with correlation coefficients greater than 0.99. It is more likely that the two isoforms of the protein, which contain Ser (Val) at position 1 and Glu (Val) at position 5 in the chicken (human) domain and are otherwise identical, possess slightly different backbone conformations. The extent of the differences was estimated using the method of Zweckstetter and Bax (2002), yielding a structural noise parameter, σ^{cone}, of ~5°–10°, corresponding to an average angle between equivalent NH bond vectors in the two proteins of 6°–12°. This can help to explain why fits of (the chicken) Fyn SH3 domain relaxation data to models of anisotropic diffusion (using the coordinates of the human protein) are unstable, as discussed in Materials and Methods. Nonetheless, the results indicate that the overall structures of the human and chicken isoforms of the Fyn SH3 domain are quite similar, and the X-ray structure has been used to interpret dynamics data in this study.

Slow time scale motions

Experiments were performed to test for the presence of large-amplitude millisecond-to-microsecond time scale motions in the least stable of the three proteins (F20V). When conformational exchange modulates the chemical shift of an ^{15}N nucleus on the millisecond-to-microsecond time scale,

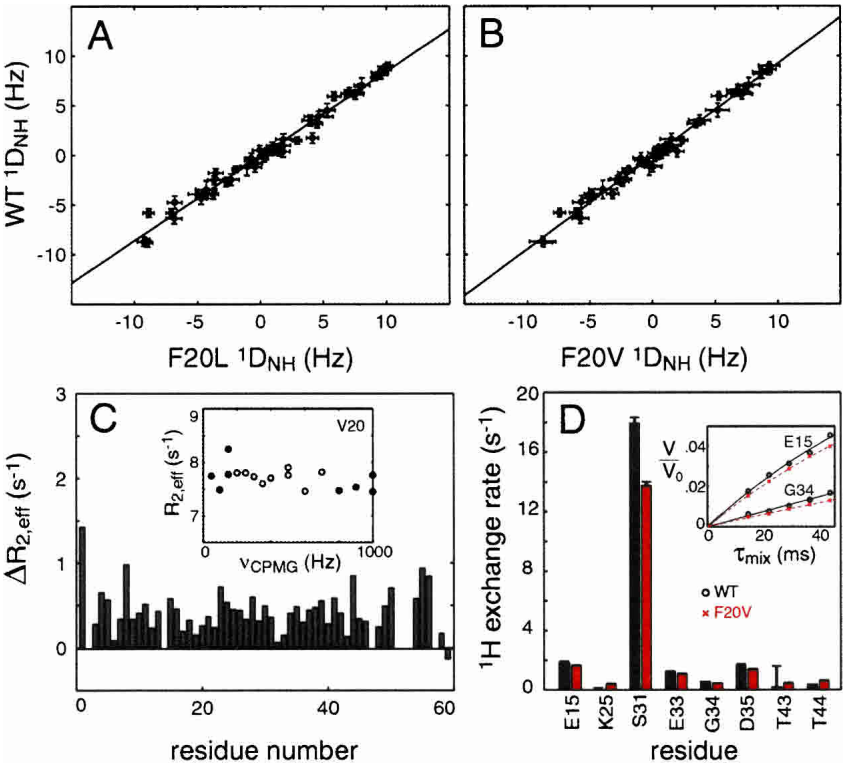

Figure 1. Comparison of one-bond ^{15}N-^{1}H residual dipolar couplings obtained for the WT SH3 domain from the Fyn tyrosine kinase with those from the F20L (*A*) and F20V (*B*) mutant proteins. Amide ^{15}N $\Delta R_{2,eff}$ values (defined in Materials and Methods) obtained for the F20V protein (*C*). Inset is the dispersion profile for Val 20 with the points used to calculate $\Delta R_{2,eff}$ identified by filled circles. Pseudo first-order rate constants for transfer of amide protons to water measured for F20V and the WT protein (*D*). Cross-peak intensities for exchange-mediated magnetization transfer are plotted as a function of mixing time for Glu 15 and Gly 34 in the inset.

the result is an increase in the effective relaxation rate of ^{15}N transverse magnetization. This contribution to R_2, termed R_{ex}, may be suppressed by the application of 180° pulses (Palmer et al. 2001). Backbone ^{15}N relaxation dispersion data were collected for F20V with CPMG 180° pulse repetition rates varying between 100 and 2000 sec^{-1} (ν_{CPMG} = 50 to 1000). A representative dispersion profile is shown in the inset to Figure 1C. Differences in $R_{2,eff}$ values between high and low ν_{CPMG} frequencies, $\Delta R_{2,eff}$, calculated as described in Materials and Methods, cluster between 0 and 1 sec^{-1} and are plotted in Figure 1C. In contrast, for the L99A mutant of T4 lysozyme, which experiences millisecond time scale exchange between a major and minor conformer (97% and 3% populated; Mulder et al. 2001), many amide resonances exhibit $\Delta R_{2,eff}$ values of 10 to 20 sec^{-1}. These data strongly indicate that large amplitude motions on the millisecond-to-microsecond time scale are not prevalent in F20V, and are unlikely to be present in F20L and the WT protein as well, although as discussed later in the text, ^{15}N $R_{1\rho}$ relaxation rates for a small number of residues in all three proteins are identified as containing R_{ex} contributions.

In addition, we have characterized the rates of amide/water hydrogen exchange for F20V and the WT protein using water magnetization transfer experiments (Hwang et al. 1998). Because ^{1}H atoms in the protein that are hydrogen bonded exchange more slowly than those that are exposed to the solvent, significant disruption of backbone hydrogen bonds in the Fyn SH3 domain would likely produce an increase in the number of sites undergoing rapid exchange. Amide protons of eight residues (E15 K25 S31 E33 G34 D35 T43 T44) show rapid exchange in one or both of the molecules. Pseudo first-order rate constants (protein to water) for these residues are plotted in Figure 1D, and show good agreement between F20V and WT, providing further evidence against a significant increase in large amplitude motions in the mutant relative to the WT protein.

Temperature dependent backbone dynamics

^{15}N $R_{1\rho}$ (Korzhnev et al. 2002), R_1 and steady-state NOE experiments (500 MHz ^{1}H frequency; Farrow et al. 1994) were recorded for uniformly ^{15}N, ^{13}C, and ≈50% ^{2}H isotopically labeled F20L, F20V, and WT protein samples at 5°, 15°, 25°, and 35°C. Relaxation data were interpreted in the context of the Lipari-Szabo Model-Free formalism (Lipari and Szabo 1982), yielding an order parameter, S^2_{NH},

per backbone amide. S^2_{NH} can take values between 1 and 0, providing a measure of the amplitude of internal dynamics that are fast on the time scale of overall tumbling with lower numbers corresponding, in general, to greater amplitudes of motion. As well, effective correlation times, $\tau_{e,NH}$ for internal motions and $\tau_{R,NH}$ for molecular tumbling in solution, were calculated for each ^{15}N-^{1}H pair for which well-resolved peaks in NMR spectra are obtained.

Based on the extracted $\tau_{R,NH}$ values, the $R_{1\rho}$ rates for several residues, (S31, A39) in WT and F20L, (E5, A39, A56) in F20V, were found to contain R_{ex} contributions, according to the approach described in Materials and Methods. This is due to either structural fluctuations involving the residues themselves or, alternatively, motions of nearby groups. In particular, the high magnetic susceptibility anisotropy of aromatic side chains modulates the chemical shifts of nearby nuclei in a conformation-dependent manner. Notably, Ser 31, Ala 39, and Ala 56 are in proximity to aromatic side chains in the WT X-ray crystal structure (Trp 37, Phe 26, and Phe 4, respectively).

In addition, Glu 33 and Gly 34 were identified as undergoing large-amplitude nanosecond time scale motions in all three forms of the protein using criteria described in Materials and Methods; in F20V, Ser 32 was implicated as well. These residues are located in the mobile N-Src loop, which is also highly dynamic in the c-Src (Wang et al. 2001) and Hck (Horita et al. 2000) SH3 domains. Extensive motion has not been detected in ^{15}N relaxation studies of SH3 domains from Btk (Hansson et al. 1998), Sem-5 (Ferreon et al. 2003), and drk (Farrow et al. 1997) proteins. Because the presence of R_{ex} and nanosecond time scale motions can compromise the reliable extraction of order parameters, ^{15}N relaxation-derived data for E5, S31, S32, E33, G34, A39, and A56 have not been included in any further analysis.

As discussed in the Appendix, the order parameter of an amide bond vector is related to its conformational entropy, S_c, with smaller values of S^2_{NH} corresponding, in general, to greater amounts of entropy. S_c/k_B values, calculated for each backbone amide according to equation 16, show temperature-dependent increases that are related to individual contributions to heat capacity, C_p, from picosecond time scale motions. Values of C_p/k_B were obtained on a per-residue basis from linear fits of S_c/k_B versus $\ln\{T\}$, as described in the Appendix, and are plotted as a function of residue in Figure 2A. C_p/k_B values cluster between approximately 1 and 3 for all three proteins, which is comparable to, although slightly lower than, results obtained for the villin head-piece protein (Vugmeyster et al. 2002) and the β1 domain from protein G (Seewald et al. 2000). In what follows, if A and B are two measurements with errors dA and dB, their difference is considered significant in cases where $|A - B| \geq 1.96(dA^2 + dB^2)^{1/2}$, which is equivalent to a 95% confidence level. In F20L, two residues (I28 and L29), and in F20V, seven residues (F4, L7, S19, F/V20, H21, I28, and Y54) show significant increases in NMR-derived heat capacity estimates relative to the WT, and representative plots of S_c/k_B versus $\ln\{T\}$ are presented in Figure 2B. No sites show a significant decrease in C_p. Order parameters for the affected residues differ in the mutant proteins compared to the WT ($S^2_{NH,F20L,V} - S^2_{NH,WT}$) by 0.024 at 5°C and by −0.021 at 35°C, on average.

We have eliminated data for residues showing obvious signs of millisecond–microsecond time scale conformational exchange or nanosecond time scale motions. Nevertheless, these processes are likely present for many residues to some extent, and can influence the extracted values of S^2_{NH}. Even if the deviations are less than the experimental uncertainty of S^2_{NH}, both R_{ex} contributions to $R_{1\rho}$ and the correlation times of nanosecond time scale motions can vary systematically with temperature. Because the changes in S^2_{NH} are very small over the range of temperatures studied here (0.02 for the WT protein on average), caution must be exercised in the interpretation of NMR-derived C_p values. It is clear, however, that regardless of the specific nature of the motions, the temperature dependence of dynamics for several residues are affected by the F20L and F20V mutations.

Magnitude of backbone motions

To characterize backbone flexibility with optimal precision, we have combined S^2_{NH} data at all four temperatures to produce a single order parameter per residue for each of the three proteins. Plots of S_c/k_B versus $\ln\{T\}$, as in Figure 2B, were interpolated at 25°C, and the values of S_c/k_B thus obtained were reconverted to order parameters, S^2_{interp}, via equation 16. S^2_{interp} values are plotted as a function of residue number in Figure 2C, showing a remarkable degree of conservation among the three proteins with correlation coefficients greater than 0.9 for both F20L and F20V data relative to those of the WT. Nonetheless, eight residues (L7, D9, E11, A12, R13, D17, F/L20, and Y54) are significantly more mobile, and three (S19, K25, and E46) less mobile in F20L compared to WT (25°C). In the case of F20V, 13 residues (L7, Y8, D9, E11, A12, R13, D17, F/V20, K22, G23, N30, T43, and Y54) show a significant increase in dynamics, and three (S19, H21, and T44) show a statistically significant decrease. Many amides in the RT-Src loop, comprising residues 7 to 24, show lower S^2_{interp} values in the mutants than in the WT protein. Thus, both F20L and F20V mutations result in increased backbone flexibility at the site of the substitutions. Slight decreases in backbone flexibility, many of which are small in relation to the experimental uncertainties, are detected for the Distal loop and the second β-strand in F20L and, to a lesser extent, in F20V, compared to the WT. These regions are also in proximity to the mutated residue, as is evident in Figure 5. The responses of backbone dynamics are quite similar for the

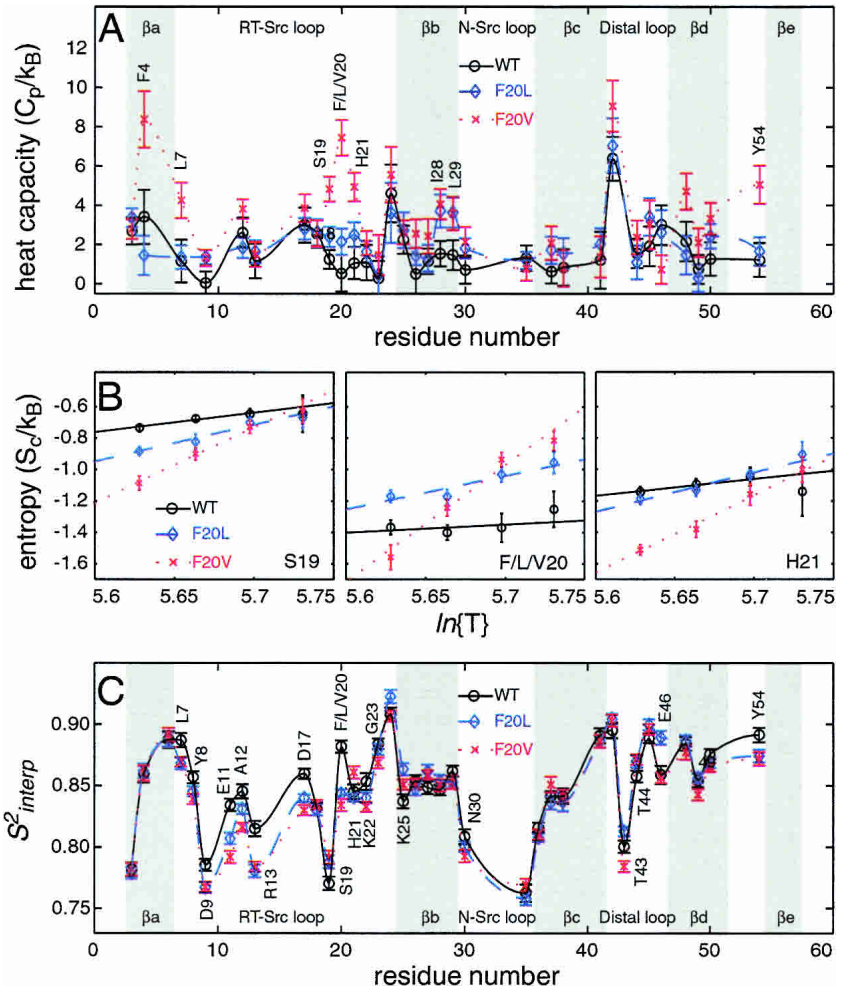

Figure 2. ^{15}N spin relaxation derived estimates of NH bond vector heat capacity (C_p/k_B, described in the text) plotted as a function of residue number for the WT SH3 domain from the Fyn tyrosine kinase and the F20L and F20V hydrophobic core mutants (*A*). Only data where linear fits of S_c/k_B vs. $ln\{T\}$ give $\chi^2 < 5$ for all proteins are included ($\chi^2 = \Sigma_{i=1}^{4}((S_c/k_B)_i - \ln\{T_i\}C_p/k_B - Y)^2/\sigma_i^2$, σ_i is the experimental uncertainty in $(S_c/k_B)_i$ measured at temperature T_i, and Y is the y-intercept). ^{15}N spin relaxation derived estimates of NH bond vector conformational entropy (S_c/k_B) for Ser 19, Phe/Leu/Val 20, and His 21 plotted as a function of temperature (T = 5°, 15°, 25°, and 35°C) for F20L, F20V, and WT proteins with linear fits indicated by dashed, dotted, and solid lines, respectively (*B*). Note that NMR-derived entropy values do not include kinetic energy contributions, and therefore can assume negative values, unlike the total entropy, which is positive for every bond vector. Backbone order parameters interpolated at 25°C from data at four temperatures plotted as a function of residue (*C*). Only residues giving rise to well-resolved peaks for all proteins at all temperatures are included.

two mutations. A comparison of ΔS^2_{interp}(F20V-WT) versus ΔS^2_{interp}(F20L-WT) values, shown in Figure 3A, has a correlation coefficient of 0.78. The probability that a correlation this strong could be observed for a sample this large (n = 37) due to chance is very low, $p = 1.4 \times 10^{-8}$.

Magnitude of side-chain motions

Experiments to measure the rates of decay of five deuterium magnetization operators (Millet et al. 2002) were performed at 25°C and 500 MHz ^{1}H frequency on the F20L, F20V, and WT protein samples that were also used for ^{15}N measurements. Relaxation rates were analyzed using the Lipari-Szabo Model-Free formalism (Lipari and Szabo 1982), generating for each methyl group an order parameter, S^2_{axis}, describing the orientational restriction of the ^{13}C-$^{13}C_{methyl}$ bond in the molecular frame. As well, an effective correlation time for internal motion, $\tau_{e,axis}$, and for molecular rotational diffusion, $\tau_{R,axis}$, was obtained for each methyl group. No conformational exchange effects were detected from an analysis of $\tau_{R,axis}$ values. Leu 42 was found to undergo large-amplitude nanosecond timecale motions in both F20L and F20V, while no ^{2}H relaxation data are available for this residue in the WT protein due to spectral overlap of both Leu 42 ^{1}H-^{13}C methyl cross-peaks. In addition, the γ1 methyl group of Val 58 shows evidence of nanosecond time scale

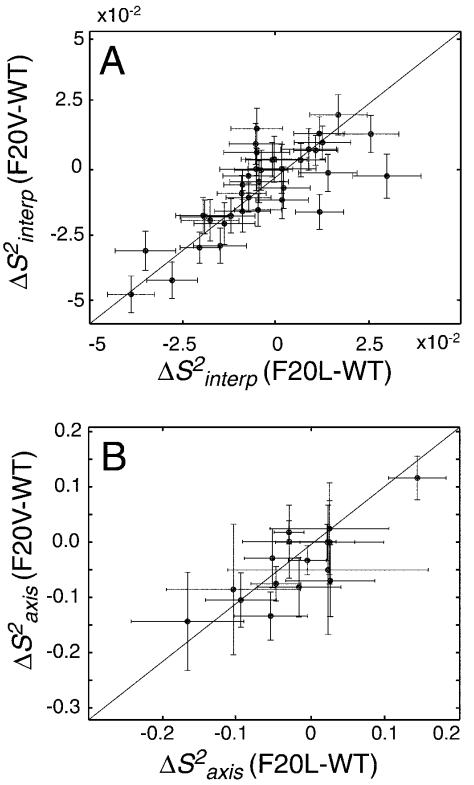

Figure 3. Comparison of changes in backbone order parameters, $\Delta S^2_{\text{interp}}$, (25°C) resulting from F20L and F20V mutations (*A*). Comparison of changes in side-chain order parameters, ΔS^2_{axis}, resulting from the F20L and F20V mutations (*B*); ΔS^2(F20X-WT) = S^2(F20X) – S^2(WT), X = L,V. Lines were fit to the data by least-squares minimization, accounting for experimental uncertainties in both dimensions.

motions in the F20V mutant; consequently, data for this residue were not included in any further analysis.

Order parameters for methyl groups where F20L, F20V, and WT data are available are plotted in Figure 4A. Similar profiles of side-chain flexibility are detected in the three molecules, and comparisons of F20L and F20V S^2_{axis} values with those of the WT give correlation coefficients greater than 0.90 for both proteins. Differences in methyl dynamics relative to the WT protein are similar for F20L and F20V. A comparison of ΔS^2_{axis}(F20V-WT) versus ΔS^2_{axis}(F20L-WT) values, shown in Figure 3B, has a correlation coefficient of 0.80 with a high statistical significance ($p = 1.5 \times 10^{-4}$). The methyl group of Thr 43 becomes significantly less mobile in both F20L and F20V compared to the WT protein. Two methyl groups in F20L (A12β and I28δ1) and three in F20V (L7d2, I28δ1, and V55γ1) show significantly more motion than in the WT protein. Overall, the F20L and F20V mutations produce slight increases in the amount of fast time scale dynamics detected for side chains. Of particular interest, five hydrophobic core positions contain methyl groups (A6, I28, A39, I50, and V55). Not considering data for the alanine residues because these report motions of the backbone, the six S^2_{axis} values of Ile 28, Ile 50, and Val 55 decrease relative to those of the WT protein by, on average, 0.057(±0.02) in F20L and 0.064(±0.03) in F20V, where brackets denote the experimental uncertainties of the mean differences. The corresponding probabilities that the observed differences could be due to chance are 1.3% and 1.7% for F20L and F20V, respectively.

Good agreement among the three proteins is obtained for effective internal correlation times, $\tau_{e,\text{axis}}$, plotted for the WT versus corresponding F20L and F20V values in Figure 4B and C. A6β, A12β, and I50γ2 are notable exceptions. Ala 12 is located in the RT-Src loop where the ^{15}N relaxation parameters of many amides indicate greater flexibility in F20L and F20V than in the WT protein. The Cβ and Cγ2 methyl carbons of Ala 6 and Ile 50, respectively, are both within 3.6 Å of the nearest Phe 20 heavy atom in the WT structure. Values of $\tau_{e,\text{axis}}$ are strongly influenced by rates of methyl rotation, particularly for larger values of S^2_{axis}, and it has been concluded in several investigations (Morishima and Iizuka 1975; Batchelder et al. 1983; Chatfield et al. 1998) that steric interactions largely determine methyl rotation rates. Changes in $\tau_{e,\text{axis}}$ are therefore likely due to slight shifting of core side chains in response to the phenylalanine to leucine and valine substitutions. The large increases in $\tau_{e,\text{axis}}$ values for A6β and I50γ2 may reflect increased intramolecular contacts involving these methyl groups. The high sensitivity of $\tau_{e,\text{axis}}$ values to structural perturbations in this study identifies them as potentially general probes of methyl environment in proteins. This is in distinct contrast to backbone internal correlation times, $\tau_{e,\text{NH}}$, which show little correlation between corresponding residues in F20L, F20V, and the WT protein.

Discussion

Amide ^{15}N- and methyl ^{2}H-NMR spin relaxation data have been used to calculate order parameters describing backbone (S^2_{interp}) and side-chain (S^2_{axis}) flexibility for the Fyn SH3 domain as well as for F20L and F20V hydrophobic core mutants. The differences in S^2_{interp} and S^2_{axis} among the three proteins are small in magnitude compared to the overall ranges of values observed for these parameters. This is consistent with a study of relatively conservative hydrophobic core substitutions in the B1 domain of protein L that found similarly small changes in fast time scale side-chain and backbone motion (Millet et al. 2003). More disruptive mutations have been reported to produce larger changes in protein dynamics. For example, the L78K sequence variant of thioredoxin shows globally decreased values of S^2_{NH} and increased R_{ex} contributions to transverse ^{15}N relaxation compared to the WT protein (DeLorimier et al. 1996). Replacement of two buried leucine residues with alanine in the four helix bundle ROP protein results in significantly in-

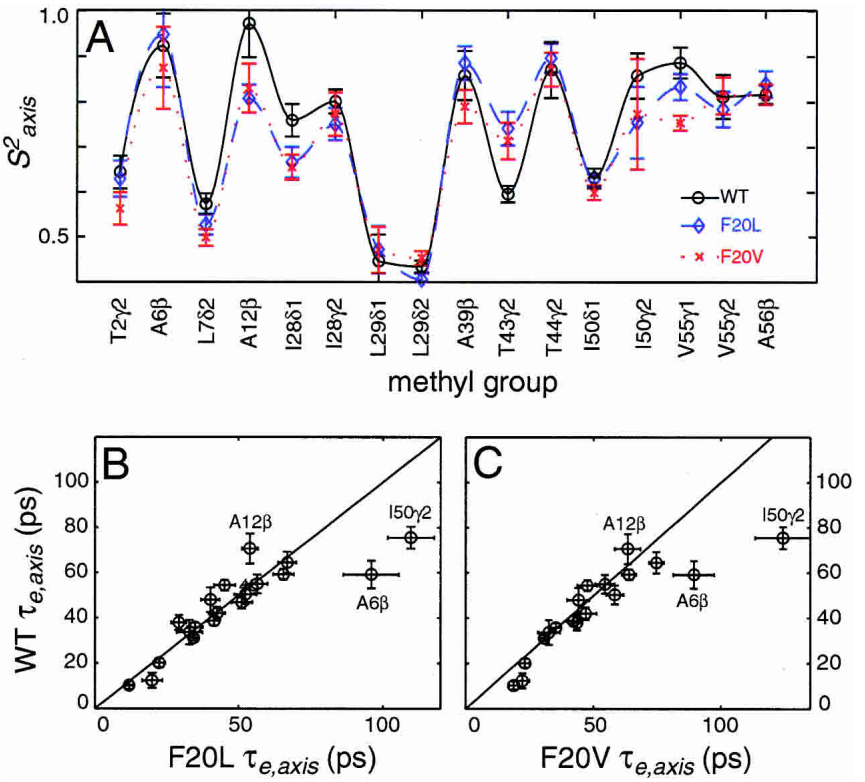

Figure 4. Methyl axis order parameters (S^2_{axis}) calculated from five experimental ^{2}H relaxation rates measured at 25°C, plotted as a function of methyl group for the WT Fyn SH3 domain and F20L and F20V hydrophobic core mutants (*A*). Comparisons of WT ^{2}H CH_2D internal correlation times, $\tau_{e,axis}$, with those of F20L (*B*) and F20V (*C*). Lines have a *y*-intercept of zero and a slope of unity. Only methyl groups with well-resolved peaks in ^{1}H-^{13}C correlation maps of all three proteins are included. Data for the WT protein have been published previously (Mittermaier et al. 2003).

creased crystallographic B-factors for atoms of core residues (Vlassi et al. 1999). A protein G β1 domain with a redesigned core 15% larger in volume than that of the WT protein has a broadened ^{1}H-NMR spectrum and more rapid exchange of amide protons with those of H_2O (Dahiyat and Mayo 1997b). With this in mind, it is interesting to note that F20V is less stable than F20L and shows greater overall backbone and side-chain mobility. The Phe to Val mutation is more disruptive than that of Phe to Leu because it introduces branching of the β-carbon and represents a larger decrease in side-chain volume.

Both the F20L and F20V hydrophobic core mutants exhibit slightly enhanced flexibility compared to the WT Fyn SH3 domain. The increases in side-chain motion are particularly notable because a strong correlation between S^2_{axis} values and measures of local packing density calculated from molecular structures was not observed for a database of eight proteins (Mittermaier et al. 1999). In this study, reduction of the volume of buried side chains correlates with increased motion, indicating that steric interactions within the hydrophobic core can influence side-chain flexibility. The effects of the mutations on dynamics are correlated such that both F20L and F20V substitutions tend to cause similar changes in the order parameter of a given amide or methyl group, providing confidence in the dynamics parameters. For the backbone, this mainly reflects the large number of residues in the RT-Src loop, which includes Phe 20, that show more mobility in F20L and F20V than in the WT. Affected side chains are distributed more globally throughout the structure, and it is not obvious why the dynamics of certain methyl groups are more sensitive to the mutations. For example, the δ1 methyl group of Ile 28 is significantly more mobile in F20L and F20V than in the WT protein and yet is more than 9 Å away from the nearest Phe 20 heavy atom.

Differences in the conformational entropy of the mutant proteins relative to that of the WT were estimated using equation 16, focussing on amide and methyl groups for which data are available in all three molecules, yielding 1.50 cal/mole/K for the backbone and 5.06 cal/mole/K for the side chains of F20L, and 3.45 cal/mole/K for the backbone and 9.36 cal/mole/K for the side chains of F20V. The corresponding changes in free energy at 25°C are −1.95 kcal/mole for F20L and −3.82 kcal/mole for F20V, summing backbone and side-chain contributions. These values are large compared to changes in the free energies of un-

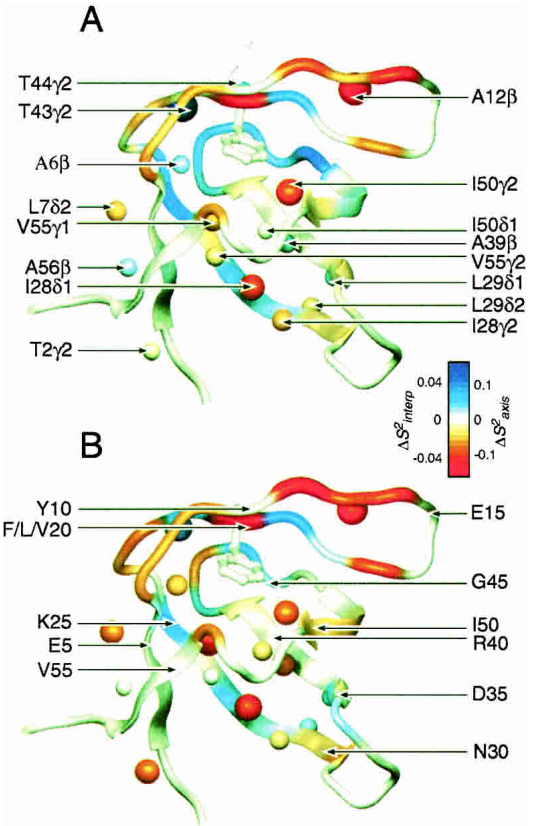

Figure 5. Differences in order parameter values relative to those of the WT Fyn SH3 domain (ΔS^2_{interp}, ΔS^2_{axis}) for F20L (*A*) and F20V (*B*) color-coded on a ribbon representation of the WT X-ray crystal structure (1SHF; Noble et al. 1993) with the locations of methyl groups for which ^2H relaxation data exist in all three proteins indicated by spheres. The mutated residue, Phe 20, is shown in ball-and-stick format. Regions of the backbone or methyl groups with increased mobility are colored red. Those with decreased mobility are colored blue. Greater changes in order parameters are indicated by more intense colors and larger radii for both the ribbon and spheres. Identities of methyl groups are indicated in (*A*) and locations of C^α atoms are shown in (*B*).

folding accompanying the substitutions, due in part to the fact that the dynamics at individual positions are probably not uncorrelated, as assumed in the analysis here. Nevertheless, it is likely that the contribution of conformational entropy to the stability of the mutant proteins is greater than for the WT.

The entropic stabilization of F20L and F20V relative to the WT implies that the changes in enthalpy accompanying the substitutions are even larger, because both mutants are less stable than the WT protein. Disruption of interactions directly involving the side chain of Phe 20 likely contribute to the destabilization of F20L and F20V. Enhanced flexibility may play an additional role by modulating the strength of interatomic contacts. For instance, Van der Waals interactions are strongly distance-dependent and could potentially be weakened by increased side-chain motion. Several ^2H relaxation studies of SH2 domain peptide binding provide evidence for a link between NMR-derived order parameters and protein energetics (Kay et al. 1998; Finerty et al. 2002). In these investigations, a positive correlation was found between the contribution made by a side chain to the affinity of an SH2 domain/ligand interaction and the extent to which its motion is quenched in the bimolecular complex. Hydrogen bonding could be similarly weakened by increased motion because the strength of these interactions depends upon the separation and orientation of donor and acceptor groups. (Note that the similar rates of amide proton exchange with water in F20V and the WT protein indicate that hydrogen bonds present in the WT also exist in the mutant.) It has been observed in a variety of systems that the typical structural response of proteins to volume-reducing hydrophobic core substitutions is subtle conformational rearrangements that minimize the size of the resultant cavities (Richards and Lim 1994). The results presented in this study, as well as those of others discussed above, indicate that proteins show a common dynamic response to disruption of the hydrophobic core as well: an enhancement of flexibility whereby the enthalpic penalty of weakening van der Waals and hydrogen bonding interactions via higher mobility is offset by an increase in entropy.

Very conservative hydrophobic core substitutions have produced detectable changes in the dynamics of the Fyn SH3 domain. Slowing of internal motions for two methyl groups (A6β and I50γ2) likely reflects increased contact of these moieties with surrounding atoms. Slight increases in the amplitudes of fast time scale dynamics are consistent with a trend of hydrophobic core perturbations leading to enhanced protein flexibility. Several amide groups with elevated NMR-derived heat capacity values in F20V and F20L show decreased flexibility compared to the WT at low temperatures and increased flexibility at higher temperatures. This surprising result highlights the unique dynamic information provided by NMR relaxation experiments and underscores the need for further investigation.

Materials and methods

Sample preparation

DNA coding for the WT and F20L and F20V sequence variants of the chicken isoform of the Fyn tyrosine kinase was obtained from the laboratory of Alan Davidson (University of Toronto), and was amplified by PCR from Val 1 to Asp 59 in the numbering scheme of Larson and Davidson (2000). The PCR product was inserted between NcoI and BglII restriction endonuclease sites in a pET11d (Novagen) expression plasmid with an ochre stop codon included in the 3′ PCR primer. Integrity of the construct was verified by DNA sequencing. Freshly transformed *Escherichia coli* BL21 DE3 cells were innoculated into 1 L of 50% ^2H_2O, M9 minimal media with $^{15}NH_4Cl$ and ^{13}C-glucose as the sole sources of nitrogen and carbon, and grown at 37°C with aeration. Protein expression was induced at an OD_{600} of 0.7 with the addition of 200 mg/L IPTG

and allowed to continue for 4 h. Cells were harvested by centrifugation, and lysis was achieved by two repetitions of sonication and centrifugation. The supernatants were applied to an anion exchange column (DE52 resin, Whatman Group) and eluted with a 0- to 1-M gradient of sodium chloride. The appropriate fractions were further purified using size-exclusion (Superdex G-75 prepacked column, Pfizer-Pharmacia) and hydrophobic interaction chromatography. The latter employed butyl-650M resin (Tosohaas, Tosoh Corp.) and a 1.2- to 0-M ammonium sulfate gradient. The protein was free from contaminants as established by overloaded SDS-PAGE and the concentration was determined by absorbance at 280 nm using a theoretical extinction coefficient predicted on the basis of the primary sequence (Pace et al. 1995). NMR experiments were performed on 1.5 mM protein samples containing 50 mM Na_3PO_4 (pH 6.0), 0.05% NaN_3, 0.2 mM EDTA, and 10% ^2H_2O at 25°C using a Varian Inova spectrometer operating at 500 MHz ^1H frequency. In cases where sample alignment was required, Pf1 bacteriophage (Hansen et al. 1998) were added to samples described above to give a final concentration of 19 mg/mL.

Data analysis

All NMR spectra were processed using the NMRPipe/NMRDraw suite of programs (Delaglio et al. 1995), and peak heights and volumes were fit using nlinLS software (Delaglio et al. 1995). ^{15}N R_1 and $R_{1\rho}$ rates (Farrow et al. 1994; Korzhnev et al. 2002) were determined from decreases in peak volume as a function of relaxation delay and experimental uncertainties in rates were estimated using the deviations of experimental values from the best-fit decay curve. NOEs were calculated as the ratio of peak heights in ^1H-^{15}N correlation spectra measured with a relaxation delay of 12 s (no NOE) or 7 sec followed by 5 sec of ^1H presaturation (NOE), and errors were estimated from spectral noise. Lipari-Szabo Model-free analysis (Lipari and Szabo 1982), was performed for β-sheet residues (3–6, 25–29, 36–41, 47–57) to yield an effective correlation time, $\tau_{R,NH}$, per amide. These values were used to fit global anisotropic rotational diffusion parameters for each protein and temperature in the quadric approximation limit (Bruschweiler et al. 1995) using the WT X-ray crystal structure of the human protein(1SHF; Noble et al. 1993) and software available from the research group of A.G. Palmer (Columbia University). The data were insufficient to precisely define the orientation of the diffusion tensor relative to the molecular structure, resulting in large experimental uncertainties (≈30°) in Euler angles. Because the choice of diffusion tensor can affect the values of extracted order parameters, we preferred to fit individual diffusive correlation times on a per-residue basis to avoid systematic errors in comparisons of order parameters between different proteins. S^2_{NH}, $\tau_{e,NH}$, and $\tau_{R,NH}$ parameters were varied in Lipari-Szabo fits for each amide bond vector at each temperature to minimize the fractional deviations of predicted and experimental relaxation measurements. Uncertainties in experimental rates were propagated to S^2_{NH} values, and in turn, to S_c/k_B, C_p and S^2_{interp} values (see below) by Monte Carlo simulations of 1000 iterations.

Five ^2H spin relaxation rates (Millet et al. 2002) were calculated per methyl group from decreases in peak volume as a function of relaxation delay, and experimental uncertainties in rates were estimated using the deviations of experimental values from the best-fit decay curve. S^2_{axis}, $\tau_{e,axis}$, and $\tau_{R,axis}$ parameters were obtained from experimental relaxation rates by nonlinear least-squares optimization; errors in the rates were propagated to the model-free parameters by Monte Carlo simulations of 1000 iterations. For the reasons discussed above, $\tau_{R,axis}$ was fit on a per-methyl basis.

Simulations in our laboratory indicate that τ_R values are significantly overestimated in the presence of conformational exchange. For example, using the global correlation time obtained for the WT protein at 25°C (3.34 nsec), an R_{ex} contribution of 2 sec^{-1} leads to overestimation of $\tau_{R,NH}$ by 1.4 nsec. In contrast, when nanosecond time scale motions are superimposed over the fast internal motions reported by S^2_{NH}, apparent τ_R parameters are significantly smaller than their true values. This effect has also been seen in the analysis of ^2H relaxation data (Millet et al. 2003). We have therefore assumed that residues undergo conformational exchange or large-amplitude nanosecond time scale motions when $\tau_{R,NH}$ and $\tau_{R,axis}$ values deviate by more than three standard deviations (σ) from the mean (μ), averaging over all $\tau_{R,NH}$ or $\tau_{R,axis}$ values of a given protein at a given temperature, with the sign of the deviation indicating either exchange or ns motions. To obtain estimates of μ and σ that are free from potential bias due to outlying points, we have employed cropped samples in which the greatest and least 20% of the data are discarded. It is straightforward to show numerically that for normally distributed data, the standard deviation of the cropped sample is, on average, 0.463 times that of the full sample, while the means of both samples are identical. In the screening procedure described above, we thus take μ to be the mean of the cropped sample and $\sigma = \sigma_{crop}/0.463$.

^{15}N-^1H residual dipolar couplings ($^1D_{NH}$) were obtained from HSQC-IPAP spectra (Yang and Nagayama 1996; Ottiger et al. 1998) collected at 25°C; peak positions were quatitated using nmrDraw. Fitting of residual dipolar couplings to the first molecule of the X-ray crystal structure (1SHF; Noble et al. 1993) was accomplished with in-house software. The quality (Q) factor was calculated according to Clore and Garrett (1999)

$$Q = \frac{\sqrt{\sum(^1D_{NH}^{predicted} - {}^1D_{NH}^{observed})^2/N}}{\sqrt{D_a^2\frac{4+3R^2}{5}}}$$

$$D_a = -\left(\frac{\mu_0}{8\pi^2}\right)\left(\frac{\hbar\gamma_N\gamma_H}{r^3}\right)A_a \qquad (1)$$

where A_a and R are the magnitude and rhombicity of the molecular alignment tensor, respectively, and N is the sample size.

^{15}N relaxation dispersion experiments (Loria et al. 1999) were performed at 25°C and 500 MHz (^1H frequency) for the F20V protein with a constant relaxation delay, T, of 40 msec and $\nu_{CPMG} = 1/(2\tau)$ values of [50, 100, 150, 200, 250, 300, 350, 400, 500, 600, 700, 800, 900, 1000] msec, where τ is the time between 180° pulses. Duplicate measurements were made for ν_{CPMG} = [150, 500, 1000] msec. $R_{2,eff}$ values were calculated according to

$$R_{2,eff} = -\ln\left\{\frac{V}{V_0}\right\}T^{-1} \qquad (2)$$

where V is the volume of a ^1H-^{15}N cross-peak obtained with a given ν_{CPMG} frequency, and V_0 is the volume of the corresponding cross-peak in an experiment with the relaxation delay, T, set to zero. $\Delta R_{2,eff}$ values are defined as

$$\Delta R_{2,eff} = \frac{1}{4}\begin{pmatrix} R_{2,eff}(50) + R_{2,eff}(100) + R_{2eff}(150)_a + R_{2,eff}(150)_b \\ -R_{2,eff}(800) - R_{2,eff}(900) - R_{2,eff}(1000)_a - R_{2,eff}(1000)_b \end{pmatrix} \qquad (3)$$

where $R_{2,eff}(\nu_{CPMG})_{a,b}$ indicates duplicate experiments.

The rates of ^{1}H exchange between water and protein amide sites in the F20V and WT proteins were studied at 25°C using the experiment of Hwang et al. (1998), employing mixing times, τ_{mix}, of [14, 22, 29, 37, 43] msec. Pseudo first-order rate constants, k_{pw}, for the transfer of amide protons to water were extracted from the mixing time dependence of ^{1}H-^{15}N cross-peak volumes, V,

$$\frac{V}{V_0} = \frac{f \cdot k_{pw}}{R_p + k_{pw}} (1 - \exp\{-(R_p + k_{pw}) \cdot \tau_{mix}\}), \quad (4)$$

where V_0 is the volume of the corresponding cross-peak in an HSQC correlation spectrum, spin relaxation of water protons is assumed to be negligable, and R_p, the effective relaxation rate of amide protons is fit together with k_{pw}. Saturation of proton magnetization is taken into account by the parameter f; values of $f = 0.71$ were obtained for both F20V and the WT protein. A given amide site was defined as undergoing rapid exchange if V/V_0 exceeded 0.01 during the mixing period.

The statistical significance of the difference between two experimental measurements, A and B, with normally distributed errors, dA and dB, was calculated from the normal deviate, Z, defined as (Zar 1984):

$$Z = \frac{|A - B|}{\sqrt{dA^2 + dB^2}}. \quad (5)$$

The probability that a value of Z as large or larger than the one observed could be obtained due to chance is calculated from twice the area of the unit normal distribution (with a mean of zero and standard deviation of one) lying above Z

$$p(Z) = \sqrt{\frac{2}{\pi}} \int_Z^\infty e^{-x^2/2} dx = 1 - \mathrm{erf}\left(\frac{Z}{\sqrt{2}}\right), \quad (6)$$

where *erf* is the error function (Press et al. 1988). A Z-value of 1.96 corresponds to $p(Z) = 0.05$ (with 2.5% of the unit normal distribution lying above 1.96 and 2.5% lying below −1.96), and thus in cases where $|A - B| \geq 1.96(dA^2 + dB^2)^{1/2}$, the difference, $|A - B|$ is considered to be significantly different from zero. For the six methyl groups of hydrophobic core residues Ile 28, Ile 50, and Val 55, Z was calculated according to

$$Z = \frac{\langle \Delta S^2_{axis} \rangle}{d\langle \Delta S^2_{axis} \rangle} \quad (7)$$

where $\langle \Delta S^2_{axis} \rangle$ is the mean difference in order parameter between either F20L or F20V and the WT protein and $d\langle \Delta S^2_{axis} \rangle$ is the experimental uncertainty of the mean difference. The statistical significance, p, of correlation coefficients, r, was calculated from the Student's t-distribution according to Press et al. (1988)

$$t = r\sqrt{\frac{N-2}{1-r^2}} \quad (8)$$

and

$$p = I_{\frac{N-2}{N-2+t^2}}\left(\frac{N-2}{2}, \frac{1}{2}\right) \quad (9)$$

where N is the sample size and I is the incomplete β function.

Acknowledgments

We thank Dr. Hue Sun Chan for helpful discussions and Dr. Alan Davidson for generously providing DNA encoding the proteins used in this study. This work was supported by a grant from the Canadian Institutes of Health Research. L.E.K. holds a Canada Research Chair in Biochemistry.

The publication costs of this article were defrayed in part by payment of page charges. This article must therefore be hereby marked "advertisement" in accordance with 18 USC section 1734 solely to indicate this fact.

Appendix

The diffusion-in-a-cone model for calculating the heat capacity of NH bond vectors

^{15}N spin relaxation-derived order parameters provide quantitative measures of the orientational restriction of NH bond vectors on a picosecond time scale. They can be related to the contributions that motions of individual amides (on this time scale) make to the total entropy and heat capacity of proteins. Here we discuss the diffusion-in-a-cone model that has been previously used in our laboratory to fit S^2_{NH} data and estimate the values of thermodynamic parameters, and briefly compare this approach to the recently described method of Vugmeyster et al. (2002).

The probability density, p, that an NH bond vector assumes a given orientation (θ,φ), is related to the potential energy, $E(\theta,\varphi)$, such that

$$p(\theta,\varphi) = \frac{\exp\left\{\frac{-E(\theta,\varphi)}{k_B T}\right\}}{\int_0^{2\pi}\int_0^{\pi} \exp\left\{\frac{-E(\theta,\varphi)}{k_B T}\right\} \sin\theta d\theta d\varphi} \quad (10)$$

where k_B is Boltzmann's constant, T is the temperature in Kelvin, and θ and φ are the polar angles of the bond vector expressed in a frame of reference rigidly attached to the protein. For convenience, the z-axis is defined to be parallel to the mean orientation of the bond vector. Ignoring contributions from kinetic energy, the conformational entropy of the bond vector is given by (Yang and Kay 1996):

$$S_c = -k_B \int_0^{2\pi}\int_0^{\pi} p(\theta,\varphi) \ln\{p(\theta,\varphi)\} \sin\theta d\theta d\varphi \quad (11)$$

and for axially symmetric motion, in which the potential energy function is independent of the angle φ, the NMR order parameter obtained from Model-free analysis of ^{15}N relaxation data is (Lipari and Szabo 1982)

$$S = \frac{1}{2}\int_0^{\pi} (3\cos^2\theta - 1) p(\theta) \sin\theta d\theta, \quad (12)$$

where it is understood that $p(\theta)$ is normalized, that is: $\int_0^{\pi} p(\theta)\sin\theta d\theta = 1$. Equations 11 and 12 have been used to derive analytical expressions relating NMR-derived order parameters to changes in free energy (Akke et al. 1993) and entropy (Li et al. 1996; Yang and Kay 1996). For example, if an NH bond vector reorients

isotropically within a cone of semiangle β ($E(\theta) = E_0$, $\theta \leq \beta$; $E(\theta) = \infty$, $\theta > \beta$),

$$p(\theta,\varphi) = (2\pi(1-\cos\beta))^{-1} \;\; \theta \leq \beta; \;\; p(\theta,\varphi) = 0, \;\; \theta > \beta, \qquad (13)$$

$$S_c = k_B \cdot \ln\{2\pi(1-\cos\beta)\}, \qquad (14)$$

$$S = \frac{1}{2}\cos\beta(1+\cos\beta), \qquad (15)$$

and

$$S_c = k_B \cdot \ln\{\pi(3-\sqrt{1+8S})\}. \qquad (16)$$

Temperature-dependent changes in order parameter values can be related to the heat capacity of the bond vector, defined according to Zemansky and Dittman (1981):

$$C_p = \left(\frac{dQ}{dT}\right)_p = \left(\frac{\partial S_c}{\partial \ln\{T\}}\right)_p = T\left(\frac{\partial S_c}{\partial T}\right)_p = \left(\frac{\partial U}{\partial T}\right)_p + \left(\frac{dW}{dT}\right)_p \qquad (17)$$

where Q is the heat absorbed by the bond vector, W is work performed by the bond vector on the surroundings, and U is the internal energy of the bond vector which, neglecting kinetic energy contributions, is $\langle E(\theta,\varphi)\rangle$. Recently, it has been proposed that NH bond vector motions are governed by an axially symmetric, temperature-independent potential energy function (Vugmeyster et al. 2002). In this approach, $(dW/dT)_p = 0$ and

$$C_p = \left(\frac{\partial U}{\partial T}\right)_p = \frac{\langle E(\theta,\varphi)^2\rangle - \langle E(\theta,\varphi)\rangle^2}{k_B T^2}. \qquad (18)$$

Equations 10 and 12 can be used to fit S^2_{NH} values obtained at two or more temperatures to parameters describing the depth and the half-width at half-height of the potential energy well (Vugmeyster et al. 2002).

It is not necessarily the case that $E(\theta,\varphi)$ is temperature-independent. In fact, potentials of mean force for NH bond vector motions calculated from molecular dynamics simulations have shown non-negligible dependence on temperature (Massi and Palmer 2003). If entropy values are known at several temperatures, then the heat capacity of the bond vector may still be calculated according to equation 17, irrespective of the temperature dependence of the potential energy function, $E(\theta,\varphi)$. Changes in $E(\theta,\varphi)$ are equivalent to work performed by the bond vector on the surroundings or vice versa. The diffusion-in-a-cone model, described above, provides a simple example of this scenario. From equations 14 and 17 it follows that

$$\frac{d\beta}{dT} = \frac{C_p}{k_B T} \cdot \frac{1-\cos\beta}{\sin\beta} \qquad (19)$$

and

$$\frac{dW}{d\beta} = k_B T \cdot \frac{\sin\beta}{1-\cos\beta} \cdot \left(1 - \frac{1}{C_p}\left(\frac{\partial U}{\partial T}\right)_p\right). \qquad (20)$$

For $S^2_{NH} = 0.8$ ($\beta = 22°$), $C_p/k_B = 3$, and $(\partial U/\partial T)_p = 0$, equations 19 and 20 give $dW/d\beta = 54$ cal/mole/degree and $d\beta/dT = 0.11$ degrees/K at 300 K. Although the model does not predict how C_p varies with temperature, plots of S_c (calculated using equation 16 and summing over all residues) versus $\ln\{T\}$ are highly linear ($R^2 = 0.977$, 0.923, 0.997, for WT, F20L, F20V), indicating that C_p is constant over the range of temperatures studied here to good approximation. Notably, the harmonic oscillator and maximum-entropy (Vugmeyster et al. 2002) models also do not predict significant variation of C_p with T over the temperature range normally studied. In the case of a quadratic potential, $E(\theta) = \alpha\theta^2$, C_p is equal to k_B for all values of α and at all temperatures (in the limit that $p(\theta = 180°) \approx 0$; Li et al. 1996; Vugmeyster et al. 2002). The maximum-entropy potential energy function proposed for NH bond vector motions also gives a nearly linear relationship between S_c and $\ln\{T\}$ ($R^2 > 0.99$ for the range of temperatures used in this study). Therefore, we have obtained C_p on a per-residue basis from linear fits of S_c/k_B (calculated using equation 16) versus $\ln\{T\}$.

NMR-derived entropy and heat capacity values must be interpreted with several caveats in mind, irrespective of how such values are calculated. First of all, NMR-derived entropy values reflect only dynamics that affect spin relaxation; motions much slower than overall tumbling or those that occur about an axis of rotation parallel to the bond vector itself will not be accounted for. For example, a recent study found that $^{13}C'$-$^{13}C^{\alpha}$ order parameters showed significantly greater temperature dependence than those of ^{15}N-^{1}H bond vectors (Wang et al. 2003). Although both parameters describe flexibility of the backbone, it is clear that the modes of internal dynamics observed are different; NMR-derived entropy and heat capacity values may depend on the type of nucleus that is used as a probe of dynamics. Second, if the internal motions of two vectors are correlated, then their combined entropy is less than the sum of their individual values. The total entropy of NH bond vectors in a protein is therefore likely to be much less than the sum of the individual NMR-derived estimates.

References

Akke, M., Bruschweiler, R., and Palmer, A. 1993. NMR order parameters and free energy: An analytic approach and application to cooperative calcium binding by calbindin D9k. *J. Am. Chem. Soc.* **115:** 9832–9833.

Batchelder, L.S., Niu, C.H., and Torchia, D.A. 1983. Methyl reorientation in polycrystalline amino acids and peptides, a ^2H NMR spin-lattice relaxation study. *J. Am. Chem. Soc.* **105:** 2228–2231.

Bax, A. 2003. Weak alignment offers new NMR opportunities to study protein structure and dynamics. *Protein Sci.* **12:** 1–16.

Bruschweiler, R., Liao, X., and Wright, P.E. 1995. Long-range motional restrictions in a multidomain zinc-finger protein from anisotropic tumbling. *Science* **268:** 886–889.

Buckle, A.M., Cramer, P., and Fersht, A.R. 1996. Structural and energetic responses to cavity-creating mutations in hydrophobic cores: Observation of a buried water molecule and the hydrophilic nature of such hydrophobic cavities. *Biochemistry* **35:** 4298–4305.

Chatfield, D.C., Szabo, A., and Brooks, B.R. 1998. Molecular dynamics of staphylococcal nuclease: Comparison of simulation with ^{15}N and ^{13}C NMR relaxation data. *J. Am. Chem. Soc.* **120:** 5301–5311.

Chothia, C. 1975. Structural invariants in protein folding. *Nature* **254:** 304–308.

Clore, G.M. and Garrett, D.S. 1999. R-factor, free R and complete cross-validation for dipolar coupling refinement of NMR structures. *J. Am. Chem. Soc.* **121:** 9008–9012.

Dahiyat, B.I. and Mayo, S.L. 1997a. De novo protein design: Fully automated sequence selection. *Science* **278:** 82–87.

———. 1997b. Probing the role of packing specificity in protein design. *Proc. Natl. Acad. Sci.* **94:** 10172–10177.

Davidson, A.R., Lumb, K.J., and Sauer, R.T. 1995. Cooperatively folded proteins in random sequence libraries. *Nat. Struct. Biol.* **2:** 856–864.

Delaglio, F., Grzesiek, S., Vuister, G.W., Zhu, G., Pfeifer, J., and Bax, A. 1995. NMRPipe: A multidimensional spectral processing system based on UNIX pipes. *J. Biomol. NMR* **6:** 277–293.

DeLorimier, R., Hellinga, H., and Spicer, L. 1996. NMR studies of structure, hydrogen exchange and main-chain dynamics in disrupted-core mutant of thioredoxin. *Protein Sci.* **5:** 2552–2565.

De Vos, S., Backmann, J., Prevost, M., Steyaert, J., and Loris, R. 2001. Hydrophobic core manipulations in ribonuclease T1. *Biochemistry* **40:** 10140–10149.

Di Nardo, A.A., Larson, S.M., and Davidson, A.R. 2003. The relationship between conservation, thermodynamic stability and function in the SH3 domain hydrophobic core. *J. Mol. Biol.* **333:** 641–655.

Eriksson, A.E., Baase, W.A., Zhang, X.J., Heinz, D.W., Blaber, M., Baldwin, E.P., and Matthews, B.W. 1992. Response of a protein structure to cavity-creating mutations and its relation to the hydrophobic effect. *Science* **255:** 178–183.

Farrow, N.A., Muhandiram, R., Singer, A.U., Pascal, S.M., Kay, C.M., Gish, G., Shoelson, S.E., Pawson, T., Forman-Kay, J.D., and Kay, L.E. 1994. Backbone dynamics of a free and phosphopeptide-complexed Src homology 2 domain studied by ^{15}N NMR relaxation. *Biochemistry* **33:** 5984–6003.

Farrow, N.A., Zhang, O., Forman-Kay, J.D., and Kay, L.E. 1997. Characterization of the backbone dynamics of folded and denatured states of an SH3 domain. *Biochemistry* **36:** 2390–2402.

Fauchere, J.L. and Pliska, V. 1983. Hydrophobic parameters π of amino acid side chains from the partitioning of N-acetyl-amino-acid amides. *Eur. J. Med. Chem.* **18:** 369–375.

Ferreon, J.C., Volk, D.E., Luxon, B.A., Gorenstein, D.G., and Hilser, V.J. 2003. Solution structure, dynamics, and thermodynamics of the native state ensemble of the Sem-5 C-terminal SH3 domain. *Biochemistry* **42:** 5582–5591.

Finerty, P.J.J., Muhandiram, R., and Forman-Kay, J.D. 2002. Side-chain dynamics of the SAP SH2 domain correlate with a binding hot spot and a region with conformational plasticity. *J. Mol. Biol.* **322:** 605–620.

Handel, T.M., Williams, S.A., and DeGrado, W.F. 1993. Metal ion-dependent modulation of the dynamics of a designed protein. *Science* **261:** 879–885.

Hansen, M.R., Mueller, L., and Pardi, A. 1998. Tunable alignment of macromolecules by filamentous phage yields dipolar coupling interactions. *Nat. Struct. Biol.* **5:** 1065–1074.

Hansson, H., Mattsson, P.T., Allard, P., Haapaniemi, P., Vihinen, M., Smith, C.I.E., and Hard, T. 1998. Solution structure of the SH3 domain from Bruton's tyrosine kinase. *Biochemistry* **37:** 2912–2924.

Horita, D.A., Zhang, W., Smithgall, T.E., Gmeiner, W.H., and Byrd, R.A. 2000. Dynamics of the Hck-SH3 domain: Comparison of experiment with multiple molecular dynamics simulations. *Protein Sci.* **9:** 95–103.

Hwang, T.L., van Zijl, P.C.M., and Mori, S. 1998. Accurate quantitation of water-amide proton exchange rates using the Phase-Modulated CLEAN chemical EXchange (CLEANEX-PM) approach with a Fast-HSQC (FHSQC) detection scheme. *J. Biomol. NMR* **11:** 221–226.

Isogai, Y., Ota, M., Fujisawa, T., Izuno, H., Mukai, M., Nakamura, H., Iizuka, T., and Nishikawa, K. 1999. Design and synthesis of a globin fold. *Biochemistry* **38:** 7431–7443.

Isogai, Y., Ota, M., Ishii, A., Ishida, M., and Nishikawa, K. 2002. Identification of amino acids involved in protein structural uniqueness: Implication for de novo protein design. *Protein Eng.* **15:** 555–560.

Johnson, E.C. and Handel, T.M. 1999. Effect of hydrophobic core packing on side chain dynamics. *J. Biomol. NMR* **15:** 135–143.

Karplus, P.A. 1997. Hydrophobicity regained. *Protein Sci.* **6:** 1302–1307.

Kay, L.E., Muhandiram, D.R., Wolf, G., Shoelson, S.E., and Forman-Kay, J.D. 1998. Correlation between binding and dynamics at SH2 domain interfaces. *Nat. Struct. Biol.* **5:** 156–163.

Korzhnev, D.M., Skrynnikov, N., Millet, O., Torchia, D.A., and Kay, L.E. 2002. An NMR experiment for the accurate measurement of heteronuclear spin-lock relaxation rates. *J. Am. Chem. Soc.* **124:** 10743–10753.

Larson, S.M., and Davidson, A.R. 2000. The identification of conserved interactions within the SH3 domain by alignment of sequences and structures. *Protein Sci.* **9:** 2170–2180.

Lee, J. and Shin, S. 2000. Theoretical studies of the response of a protein structure to cavity-creating mutations. *Biophys. J.* **78:** 1665–1671.

Li, Z., Raychaudhuri, S., and Wand, A.J. 1996. Insights into the local residual entropy of proteins provided by NMR relaxation. *Protein Sci.* **5:** 2647–2650.

Lipari, G. and Szabo, A. 1982. Model-free approach to the interpretation of nuclear magnetic relaxation in macromolecules: 1. Theory and range of validity. *J. Am. Chem. Soc.* **104:** 4546–4559.

Loria, P.J., Rance, M., and Palmer, A.G. 1999. A relaxation-compensated Carr-Purcell-Meiboom-Gill sequence for characterizing chemical exchange by NMR spectroscopy. *J. Am. Chem. Soc.* **121:** 2331–2332.

Massi, F. and Palmer, A.G.I. 2003. Temperature dependence of NMR order parameters and protein dynamics. *J. Am. Chem. Soc.* **125:** 11158–11159.

Millet, O., Muhandiram, R., Skrynnikov, N., and Kay, L.E. 2002. Deuterium spin probes of side-chain dynamics in proteins. 1. Measurement of five relaxation rates per deuteron in ^{13}C-labeled and fractionally ^{2}H-enriched proteins in solution. *J. Am. Chem. Soc.* **124:** 6439–6448.

Millet, O., Mittermaier, A., Baker, D., and Kay, L.E. 2003. The effects of mutations on motions of side-chains in protein L studied by ^{2}H NMR dynamics and scalar couplings. *J. Mol. Biol.* **329:** 551–563.

Mittermaier, A., Kay, L.E., and Forman-Kay, J.D. 1999. Analysis of deuterium relaxation-derived methyl axis order parameters and correlation with local structure. *J. Biomol. NMR* **13:** 181–185.

Mittermaier, A., Davidson, A.R., and Kay, L.E. 2003. Correlation between 2H NMR side-chain order parameters and sequence conservation in globular proteins. *J. Am. Chem. Soc.* **125:** 9004–9005.

Morishima, I. and Iizuka, T. 1975. Nuclear magnetic resonance studies of hemoproteins. IV. Hindered rotation of heme side methyl group as a probe for studying van der Waals contacts in the heme side environments of myoglobin derivatives. *Biochim. Biophys. Acta* **386:** 542–555.

Morton, C., Pugh, D., Brown, E., Kahman, J., Renzoni, D., and Campbell, I. 1996. Solution structure and peptide binding of the SH3 domain from human Fyn. *Structure* **4:** 705–714.

Mulder, F.A.A., Mittermaier, A., Hon, B., Dahlquist, F.W., and Kay, L.E. 2001. Studying excited states of proteins by NMR spectroscopy. *Nat. Struct. Biol.* **8:** 932–935.

Musacchio, A., Wilmanns, M., and Saraste, M. 1994. Structure and function of the SH3 domain. *Prog. Biophys. Mol. Biol.* **61:** 283–297.

Noble, M.E., Mussachio, A., Saraste, M., Courtneidge, S.A., and Wierenga, R.K. 1993. Crystal structure of the SH3 domain in human Fyn; Comparison of the three-dimensional structures of SH3 domains in tyrosine kinases and spectrin. *EMBO J.* **12:** 2617–2624.

Northey, J.G.B., Di Nardo, A.A., and Davidson, A.R. 2002. Hydrophobic core packing in the SH3 domain folding transition state. *Nat. Struct. Biol.* **9:** 126–130.

Offredi, F., Dubail, F., Kischel, P., Sarinski, K., Stern, A.S., Vand de Weerdt, C., Hoch, J.C., Prosperi, C., Francois, J.M., Mayo, S.L., et al. 2003. De novo backbone and sequence design of an idealized α/β barrel protein: Evidence of a stable tertiary structure. *J. Mol. Biol.* **325:** 163–174.

Ottiger, M., DeLaglio, F., and Bax, A. 1998. Measurement of J and dipolar couplings from simplified two dimensional NMR spectra. *J. Mag. Reson.* **131:** 373–378.

Pace, C.N., Vajdos, F., Fee, L., Grimsley, G., and Gray, T. 1995. How to measure and predict the molar absorption coefficient of a protein. *Protein Sci.* **4:** 2411–2423.

Palmer, A.G., Kroenke, C.D., and Loria, J.P. 2001. NMR methods for quantifying microsecond-to-millisecond motions in biological macromolecules. *Methods Enzymol.* **339:** 204–238.

Press, W.H., Flannery, B.P., Teukolsky, S.A., and Vetterling, W.T. 1988. *Numerical recipes in C*. Cambridge University Press, Cambridge, UK.

Richards, F. and Lim, W. 1994. An analysis of packing in the protein folding problem. *Q. Rev. Biophys.* **26:** 423–498.

Richards, F.M. 1974. The interpretation of protein structures: Total volume, group volume distributions and packing density. *J. Mol. Biol.* **82:** 1–14.

Seewald, M.J., Pichumani, K., Stowell, C., Tibbals, B.V., Regan, L., and Stone, M.J. 2000. The role of backbone conformational heat capacity in protein stability: Temperature dependent dynamics of the B1 domain of Streptococcal protein G. *Protein Sci.* **9:** 1177–1193.

Vlassi, M., Cesareni, G., and Kokkinidis, M. 1999. A correlation between loss of hydrophobic core packing interactions and protein stability. *J. Mol. Biol.* **285:** 817–827.

Vugmeyster, L., Trott, O., McKnight, J., Raleigh, D.P., and Palmer, A.G. 2002. Temperature-dependent dynamics of the villin headpiece helical subdomain, an unusually small thermostable domain. *J. Mol. Biol.* **320:** 841–854.

Wang, C., Pawley, N.H., and Nicholson, L.K. 2001. The role of backbone motions in ligand binding to the c-Src SH3 domain. *J. Mol. Biol.* **313:** 873–887.

Wang, T., Cai, S., and Zuiderweg, E.R.P. 2003. Temperature dependence of anisotropic protein backbone dynamics. *J. Am. Chem. Soc.* **125:** 8639–8643.

Woolfson, D.N. 2001. Core-directed protein design. *Curr. Opin. Struct. Biol.* **11:** 464–471.

Yang, D. and Kay, L.E. 1996. Contributions to conformational entropy arising from bond vector fluctuations measured from NMR-derived order parameters: Application to protein folding. *J. Mol. Biol.* **263:** 369–382.

Yang, D. and Nagayama, K. 1996. A sensitivity-enhanced method for measuring heteronuclear long-range coupling constants from the displacement of signals in two 1D subspectra. *J. Magn. Reson. Ser. A* **118:** 117–121.

Zar, Z.H. 1984. *Biostatistical analysis*. Prentice-Hall Inc., Englewood Cliffs, NJ.

Zemansky, M.W. and Dittman, R.H. 1981. *Heat and thermodynamics*, 6th ed. McGraw-Hill, New York.

Zweckstetter, M. and Bax, A. 2002. Evaluation of uncertainty in alignment tensors obtained from dipolar couplings. *J. Biomol. NMR* **23:** 127–137.